Journal Pre-proofs

Enhancement of cadmium removal by oxygen-doped carbon nitride with molybdenum and sulphur hybridization

Jing Su, Lei Bi, Chen Wang, Tao Lyu, Gang Pan

Please cite this article as: J. Su, L. Bi, C. Wang, T. Lyu, G. Pan, Enhancement of cadmium removal by oxygen-doped carbon nitride with molybdenum and sulphur hybridization, *Journal of Colloid and Interface Science* (2019), doi: https://doi.org/10.1016/j.jcis.2019.08.104

This is a PDF file of an article that has undergone enhancements after acceptance, such as the addition of a cover page and metadata, and formatting for readability, but it is not yet the definitive version of record. This version will undergo additional copyediting, typesetting and review before it is published in its final form, but we are providing this version to give early visibility of the article. Please note that, during the production process, errors may be discovered which could affect the content, and all legal disclaimers that apply to the journal pertain.

Enhancement of cadmium removal by oxygen-doped carbon nitride with molybdenum and sulphur hybridization

Jing Su [a,d], Lei Bi *[a], Chen Wang [a,d,e], Tao Lyu [b,c], Gang Pan *[a,b,c,d,e]

[a] *Key Laboratory of Environmental Nanotechnology and Health Effects, Research Center for Eco-Environmental Sciences, Chinese Academy of Sciences, Beijing 100085, P. R. China*

[b] *School of Animal, Rural, and Environmental Sciences, Nottingham Trent University, Brackenhurst Campus, NG25 0QF, UK*

[c] *Centre of Integrated Water-Energy-Food studies (iWEF), Nottingham Trent University, Nottinghamshire, NG25 0QF, UK*

[d] *University of Chinese Academy of Sciences, Beijing 100049, P. R. China*

[e] *Sino-Danish College of University of Chinese Academy of Sciences, Beijing 100049, P. R. China*

Authors: Jing Su, e-mail: sujingwendy@hotmail.com

Chen Wang, e-mail: catherineb612@foxmail.com

Tao Lyu, e-mail: tao.lyu@ntu.ac.uk

Corresponding authors: * Gang Pan, Phone: +86-10-62849686; e-mail: gpan@rcees.ac.cn (G. Pan)

* Lei Bi, Phone: +86-10-62943436; e-mail: leibi@rcees.ac.cn (L. Bi)

Declaration of interest: none.

19   **Abstract**

20   Graphitic carbon nitride, as a popular material in the field of environmental remediation, still

21   suffers from unsatisfactory performance for heavy metals adsorption owing to lack of specific

22   adsorption sites. In this study, molybdenum (Mo) and sulphur (S) were simultaneously introduced

23   onto the surface of oxygen-doped graphitic carbon nitride (OCN) for the enhancement of Cd^{2+}

24   adsorption. The synthesized MOS/OCN-1 exhibited substantially increased maximum adsorption

25   capacity of 293.8 mg/g, calculated from Sips isotherm model, which was 8.7 times higher than that

26   for pristine OCN (33.9 mg/g). The adsorption efficiency of MOS/OCN-1 was >94% even under high

27   concentration of coexisting ions (ie. Ca^{2+}, Mg^{2+} and Zn^{2+}). MoO_3 and MoS_2 on the surface of OCN

28   were proven to interact with Cd^{2+} by forming $CdMoO_4$ and CdS species. OCN provided a stable matrix

29   with a large surface area making more active sites exposed, which greatly facilitated Mo(IV)

30   oxidation and Cd^{2+} precipitation. Our findings revealed that as well as the well-known Cd-S

31   interaction, Mo atoms in the hybrid composites also played an important role in Cd^{2+} removal, which

32   opened up the application possibility of OCN with Mo and S hybridization for *in-situ* Cd^{2+}

33   remediation.

34   **Keywords:** Cadmium adsorption; graphitic carbon nitride; heavy metals removal; molybdenum

35   compound; nano material

36

37   **1. Introduction**

38   Over the past decades, cadmium (Cd^{2+}) contamination of farmland and natural waters has

39   been of increasing concern due to its high toxicity and persistence [1, 2]. In some cases,

40   contamination has led to deleterious effects on the human health, including reproductive disorder,

41 liver damage or carcinogenicity, when cadmium, even at trace concentrations, entered into human

42 bodies through the food web [1, 3-6]. Adsorption has long been considered as a promising method

43 for the remediation of Cd^{2+} polluted soils and waters due to its characteristics of low cost, high

44 efficiency and simple operation when compared with other techniques such as flocculation,

45 membrane filtration, biological remediation and electrochemical treatment [2, 7]. Hence, in order

46 to ensure food and drinking water safety, the exploration of efficient adsorbents for Cd^{2+} removal is

47 an urgent need.

48 Graphitic carbon nitride (g-C_3N_4) is a carbon based material with graphene-like structure,

49 which has attracted much attention for the degradation of organic pollutants due to its

50 semiconductor properties, long-term stability and environmental friendliness [8]. Several studies

51 have also proven the efficacy of bulk g-C_3N_4 for the removal of heavy metals, e.g. Cd(II), Pb(II), Cu(II),

52 Ni(II) and Cr(VI), but only modest adsorption capacities have been achieved [6, 9, 10], since the

53 relative less active sites of bulk g-C_3N_4 hinder the achievement of higher adsorption efficiency [11].

54 In order to improve the adsorption ability towards heavy metals, several studies attempted to

55 introduce new active sites onto the bulk g-C_3N_4. Zou et al [12] modified β-cyclodextrin on g-C_3N_4

56 and the synthesized compounds exhibited a significantly improved adsorption capacity towards Pb^{2+}

57 due to the induced oxygen-containing groups. Wang et al [13] decorated g-C_3N_4 with

58 polyethyleneimine in order to increase the number of functional groups (C-C, C-O, N-C=C, etc), and

59 the modified material performed superior complexation of U(VI) and Am-243(III). Moreover,

60 enlarging the surface area of the adsorbent may further enhance the adsorption capacity by

61 providing additional adsorption sites. Qiu et al [14] reported that the oxygen-doping of graphic

62 carbon nitride (OCN) could substantially increase the surface area of g-C_3N_4 and facilitate the

63   adsorption of organic pollutants. However, OCN hasn't yet been tested for the adsorption of heavy

64   metals. We hypothesize that modification of OCN by inclusion of active groups might overcome the

65   challenges of limited adsorption active sites and surface area, enabling more effective Cd^{2+} removal.

66   It is well known that S^{2-}/-HS are effective groups for the capture of heavy metals due to strong

67   soft-soft interactions with heavy metals according to Pearson's theory [15, 16]. MoS_2, as one of the

68   typical molybdenum compounds with a large amount of intrinsic sulphur, has been proven to be a

69   promising adsorbent for the removal of Hg^{2+} [17, 18], Pb^{2+} [19], and Cd^{2+} [20]. Intensive studies have

70   shown that disulphide (S-S) planes in MoS_2 are active, and that S^{2-} can act as soft base to form M-S

71   complex with Hg/Pb/Cd soft acid through electron interaction and covalent bonding [17, 18, 20]. As

72   a comparison, the direct effects and mechanisms of Mo atoms on Cd^{2+} adsorption are rarely

73   investigated. Several studies demonstrated that MoS_2 is thermodynamically unstable in the aerobic

74   and high moisture conditions, where Mo(IV) is likely to be oxidized to Mo(VI), such as MoO_3 [21,

75   22]. The oxidized Mo(VI) has been demonstrated to be able to immobilize Pb^{2+}/Hg^{2+} by forming

76      $PbMoO_4$ or a Mo-O-Hg complex [23, 24]. Since the similar soft-acidic property of Cd^{2+} is shared by

77   Hg^{2+} and Pb^{2+}, different valencies of Mo may also influence the adsorption behaviour for Cd^{2+}. Thus,

78   these mechanisms, particularly the possibly synergistic effects of Mo and S, for improving Cd^{2+}

79   removal are in need of investigation.

80   In this study, we prepared oxygen-doped graphitic carbon nitride (OCN) and then

81   simultaneously introduced Mo and S on the surface via a facile hydrothermal method, to produce

82   the hybrid adsorbent (MOS/OCN) which was considered suitable for Cd^{2+} removal. In order to

83   evaluate the enhanced Cd^{2+} adsorption performance, MOS/OCN was optimized and the adsorption

84   capacity was compared to pristine OCN, MoS_2 and other published adsorbents. The adsorption

85   kinetics and isotherm were evaluated to address the adsorption behaviours of Cd^{2+}. The anti-

86   interference ability of MOS/OCN was also investigated under the coexistence of competitive ions,

87   i.e. Ca^{2+}, Mg^{2+} and Zn^{2+}, during Cd^{2+} removal. Lastly, in order to elucidate the adsorption mechanisms

88   of Cd^{2+}, the effects of Mo (IV /VI) and S atoms on the Cd^{2+} adsorption process were further assessed.

89   With these results, this study aims to suggest a new effective adsorbent for Cd^{2+} removal with an

90   explanation of fundamental mechanisms involved.

2. Materials and Methods

2.1 Reagents

93   Urea (>99%), oxalic acid dehydrate (≥99.5%), ammonium molybdate tetrahydrate ($(NH_4)_6$

94    $Mo_7O_{24}\cdot4H_2O$, >99%), thiourea (> 99%) and metal nitrate (Cd(II), Zn(II), Mg(II), Ca(II), > 99%) were

95   purchased from Sinopharm Chemical Regent Co. Ltd. N, N-Dimethylformamide (DMF, > 99.8%) was

96   obtained from J&K Chemical Reagent Co., Ltd. Deionized water was used in all experiments.

2.2 Synthesis of Adsorbents

2.2.1 Synthesis of oxygen-doped graphitic carbon nitride (OCN)

99   The OCN was synthesized according to Qiu et al, 2017 [14] with slight modification. Briefly,

100   urea (10 g) and oxalic acid dehydrate (4 g) were mixed by grinding in a mortar. The mixture powder

101   was then transferred into a quartz boat and calcined at 550°C for 4 h with a heating rate of 3°C/min

102   in an atmosphere of N_2.

2.2.2 Synthesis of MOS/OCN-x hybrid composites

104   Firstly, OCN (80 mg) was added into pre-mixed solution composed of DMF (64 mL) and

105   deionized water (16 mL) and sonicated for 1 h to form a homogeneous solution. Then, a required

106   amount of $(NH_4)_6Mo_7O_{24}\cdot4H_2O$ and thiourea were added into this mixed solution and stirred at

107 60°C for 30 min to ensure those reagents were totally dissolved. The molar ratio of $(NH_4)_6Mo_7O_{24}$

108 $\cdot 4H_2O$ and thiourea was kept in constant of 1:30. The mixture was further sonicated for 1h and

109 then transferred into 100 mL Teflon stainless steel autoclave and heated to 180°C for 18 h. After

110 cooling down to ambient temperature, the solid samples were collected by centrifugation and

111 washed sequentially three times with deionized water and absolute ethyl alcohol. Finally, the solid

112 was dried at 60°C for 12 h in the vacuum oven. The ultimate sample was denoted as MOS/OCN-x,

113 where x equalled to 0.5, 1, 2 and 4 when the mass ratio of $(NH_4)_6Mo_7O_{24} \cdot 4H_2O$ to OCN was

114 0.5:1, 1:1, 2:1 and 4:1, respectively. Molybdenum disulphide, named as MOS-DMF, was also

115 prepared by this procedure but without addition of OCN.

116 **2.2.3 Synthesis of MoO₃/OCN**

117 The pure MoO₃ was prepared via a facile hydrothermal reaction, according to Liu et al., 2016

118 [25]. Then, a required amount of MoO₃ powder, of which the total Mo was equal to that of

119 MOS/OCN-1 was ground with OCN (80 mg) by mortar and pestle for 30 min and added into solution

120 composed of DMF (64 mL) and H_2O (16 mL) for further sonication treatment (1 h). The mixed

121 solution was transferred into 100 mL Teflon-lined autoclave and heated to 180°C for 18 h. The

122 synthesized MoO₃/OCN solid was then collected and dried under vacuum at 60°C.

123 **2.3 Adsorption experiments**

124 In order to determine the optimal composition of MOS/OCN, the Cd^{2+} adsorption capabilities

125 by MOS/OCN-x (x=0.5, 1, 2, 4), MOS-DMF, and OCN were evaluated. In the adsorption experiment,

126 adsorbent (5 mg) was added into Cd^{2+} solution (20 mL) with an initial concentration of 20 mg/L. The

127 mixture was then agitated at 130 rpm for 24 h under 25°C. The solution pH was kept at 6.0 ± 0.2 by

128 adding 0.1 M HNO₃ or 0.1 M NaOH. After the reaction, 3 mL supernatant was collected and filtered

129   through 0.22 μm pore size membrane for determination of Cd^{2+} concentration.

130   The optimal MOS/OCN-1 was further utilised in the Cd^{2+} removal kinetics and isotherm

131   experiments in order to evaluate adsorption behaviours. For the kinetics experiment, dosages of

132   0.25 g/L MOS/OCN-1, MOS-DMF, and OCN were separately added to Cd^{2+} solution (20 mg/L, 20 mL)

133   at constant pH (6.0 ± 0.2) and temperature (25°C). During the experiment, the suspensions were

134   collected from 0-36 h to determine the Cd^{2+} concentration. Pseudo-first order, pseudo-second order

135   and intraparticle diffusion models were used to simulate experimental data (Supporting Information,

136   S1). The adsorption isotherm study was further performed to determine the maximum Cd^{2+}

137   adsorption capacity. Briefly, MOS/OCN-1, MOS-DMF, and OCN (each 5 mg) were separately added

138   into Cd^{2+} solution (20 mL) with initial concentrations of 15-600 mg/L at pH 6.0 ± 0.2 and 25 °C. After

139   24 h, the supernatant was taken for analysis of Cd^{2+} concentration. Langmuir, Freundlich and Sips

140   isotherm models were conducted to simulate the experimental data (Supporting Information, S1).

141   The Cd^{2+} removal efficiency and the adsorption capacity were calculated as followings:

142
$$\eta = \frac{(C_0 - C_e)}{C_0} \times 100\% \qquad (1)$$

143
$$q_e = \frac{(C_0 - C_e) \times V}{m} \qquad (2)$$

144   Where η (%) is Cd^{2+} removal efficiency, C_0 and C_e are the initial and equilibrium concentration of Cd^{2+} in

145   solution (mg/L), respectively. q_e (mg/g) is Cd^{2+} adsorption capacity in equilibrium state, V is the volume of

146   Cd^{2+} solution and m is the mass of adsorbents.

147   In order to evaluate the effect of pH on the Cd^{2+} adsorption by the optimal adsorbent

148   MOS/OCN-1, the adsorption capacity was determined under different pH values of 2, 3, 4, 5, and 6

149   with an initial Cd^{2+} of 20 mg/L. In addition, the effect of competing cations on Cd^{2+} adsorption was

150 also evaluated. During the adsorption experiment, the ions Ca^{2+}, Mg^{2+}, and Zn^{2+}, at concentrations

151 of 0, 10, 50, and 100 mg/L were added separately into the Cd^{2+} solutions (10 mg/L) and the finial

152 Cd^{2+} was analyzed. To further confirm the selectivity and anti-interference ability of MOS/OCN-1

153 towards Cd^{2+}, the mixed solution contained Cd^{2+}, Ca^{2+}, Mg^{2+} and Zn^{2+} in which each cation ion was

154 10 mg/L, was treated by MOS/OCN-1 (0.25 g/L) followed the same procedure of the adsorption

155 experiment. The remnant cation ions were determined after 24 h for the further removal efficiency

156 and distribution coefficient calculation. The distribution coefficient K_d (mL/g), a measurement of

157 affinity and selectivity [26] for each cation ions was calculated according to Equation (3):

158
$$K_d = \frac{V(C_0 - C_f)}{m} \frac{}{C_f} \tag{3}$$

159 Where C_0 and C_f (mg/L) represent the initial and equilibrium concentrations of the ions, V is the solution

160 volume (mL) and m (mg) is the mass of adsorbent.

161 To investigate the reusability of the adsorbent, the Cd^{2+} loaded MOS/OCN-1 was used for the

162 Cd^{2+} desorption and re-adsorption experiments. To initiate the desorption process, HNO_3 (250 mL,

163 0.1M) were added to the residue adsorbent solid (62.5 mg) and mixture was then shaken at 130

164 rpm at 25°C for 2h. At the end of the desorption test, the residue MOS/OCN-1 was collected and

165 dried at 60 ℃ for 24 h for the further re-adsorption study. The re-adsorption test was performed

166 in 50 mL centrifuge tubes contained MOS/OCN-1 (0.25g/L) and Cd^{2+} solution (10 mg/L) with pH kept

167 at 6. The Cd^{2+} concentration was determined after each adsorption-desorption cycle.

168 To further discover how different valencies of Mo atoms may affect Cd^{2+} adsorption, the

169 removal efficiency of Cd^{2+} by MoO_3/OCN was compared with MOS/OCN-1. The adsorbent dosage,

170 initial Cd^{2+} solution and environmental conditions were the same as previously described. All the

171 aforementioned adsorption experiments were conducted in duplicate and each sample analysis was

172   conducted in triplicate.

2.4 Sample analysis

2.4.1 Water samples analysis

175   All water samples were filled through a 0.22 µm cellulose acetate membrane and acidized by

176   1% HNO_3 before analysis. The concentration of Cd^{2+}, the leached MoO_4^{2-} and dissolved total S in the

177   filtrate was determined by inductively coupled plasma-optical emission spectrometer (ICP-OES;

178   Optima 8300, Perkin Elmer Inc., USA) with a detection limit of 0.2 mg/L. It should be noted that the

179   inductively coupled plasma-mass spectroscopy (ICP-MS; 7500a, Agilent Inc. USA) was used to

180   confirm the results when the concentration level below 0.2 mg/L.

2.4.2 Adsorbents characterization

182   The adsorbent structure and crystal phase were recorded by X-ray diffraction (XRD) patterns

183   using a PANalytical X'Pert PRO powder diffraction system (Malvern Panalytical, Cambridge, UK) with

184   Cu K_α radiation (λ=1.5418Å) and scanning speed of 5°/min from 5°-90°/2θ. The morphology of

185   adsorbents was examined by field emission scanning electron microscopy (FESEM; Su-8020, Hitachi,

186   Japan) with an acceleration voltage of 35 kV. X-ray photoelectron spectroscopy data (XPS;

187   SCALAB250Xi, Thermo Fisher Scientific, USA) was collected with a monochromatic Al K_α radiation

188   source (1486.6 eV). The specific surface areas of the original synthesized adsorbents were detected

189   according to the Brunauer-Emmett-Teller (BET) method (Micromeritics ASAP 2020 Analyzer, Mack

190   instruments, Inc., USA). Before BET measurement, the samples were degassed at 80℃ for 6 h.

191   Moreover, the characteristics of the surface functional groups presented on the adsorbents were

192   investigated on a Fourier transform infrared spectra (FTIR; Nicolet 8700, Thermo Fisher Scientific,

193   USA) with the wavenumber of 4000-400 cm^{-1}.

194 **3. Results and discussion**

195 **3.1 Characterization and optimization of adsorbents**

196 After synthesis, the XRD patterns of MOS/OCN-x, MOS-DMF, and OCN were analyzed (Fig. 1a).

197 The original OCN exhibited clear diffraction peak at $2\theta= 27.2°$ ascribed to the (002) plane of $g\text{-}C_3N_4$

198 [14]. The peak intensity decreased along with the increased mass of Mo and S hybridization

199 (increased x value) for MOS/OCN-x, which was attributed to relatively low content of OCN. For MOS-

200 DMF, the two peaks at 9.34° and 18.44° represented (001) and (002) plane of MoS_2 , which were

201 split from the pristine (002) plane of 14.13°, suggesting that the new lamellar structure had been

202 formed due to relatively low hydrothermal temperature at 180°C [27, 28]. Two other peaks at 32.87°

203 and 57.71° can be indexed to the (100) and (110) planes of MoS_2 (JCPDS card No. 075-1539),

204 respectively. Therefore, MoS_2 was confirmed to be the main composition of MOS-DMF. Besides

205 characteristic peaks of MoS_2, peaks attributable to the (310) and (430) planes of MoO_3 (JCPDS card

206 no. 21-0569) emerged in the hybrid composite of MOS/OCN-x and became more obvious when x

207 decreased to 0.5 or 1, which probably because the moderate content of OCN presented in that

208 material and facilitated the transformation of MoS_2 to MoO_3 during synthesis process. Therefore, it

209 is suggested that both MoS_2 and MoO_3 coexisted on the OCN surface in compounds MOS/OCN-x,

210 especially when x < 2, while MOS-DMF mainly comprised MoS_2.

211 OCN exhibited much higher BET surface area (74.4 m^2/g) than MOS-DMF (24.7 m^2/g).

212 Corresponding with the increasing incorporation of Mo and S onto OCN, the surface areas of these

213 adsorbents significantly decreased from 74.8 m^2/g for MOS/OCN-0.5 to 21.8 m^2/g for MOS/OCN-4

214 (Table S1). Conventionally, a large specific surface area of an adsorbent could potentiate the

215 removal abilities by providing more reaction sites [29]. In this study, this was supported by the

216 results that the adsorption capacity decreased from 68.0 mg/g for MOS/OCN-1 to 24.3 mg/g for

217 MOS-DMF with commensurate decreases in BET surface area (Fig.1b). However, OCN and

218 MOS/OCN-0.5 showed unsatisfactory adsorption performances although both of them exhibited

219 high specific surface areas. The limited adsorption capacities of OCN and MOS/OCN-0.5 probably

220 resulted from the lack of sufficient active species, such as Mo and S. Thus, the synergistic effects of

221 both the specific surface area and the number of active sites contributed to effective Cd^{2+} removal.

222 By control of the hybridization amount of Mo and S on the surface of OCN, the synthesized

223 adsorbent MOS/OCN-1 possessed the largest Cd^{2+} adsorption capacity and was thus selected as the

224 optimum adsorbent.

225 Differing morphologies of MOS-DMF and MOS/OCN-1 were also observed. The FESEM images

226 of MoS_2-DMF showed MoS_2 nanoparticles stacked layer by layer, exhibiting severe agglomeration

227 (Fig.S1a). However, for MOS/OCN-1, the edge of the hybrid composite became wrinkled and several

228 nanosheets of MoS_2 and MoO_3 erected separately (Fig. S1b), which indicated that OCN might

229 effectively retard the agglomeration of active particles, thus possibly leading to the exposure of

230 more suitable active sites and further enhancement of Cd^{2+} removal.
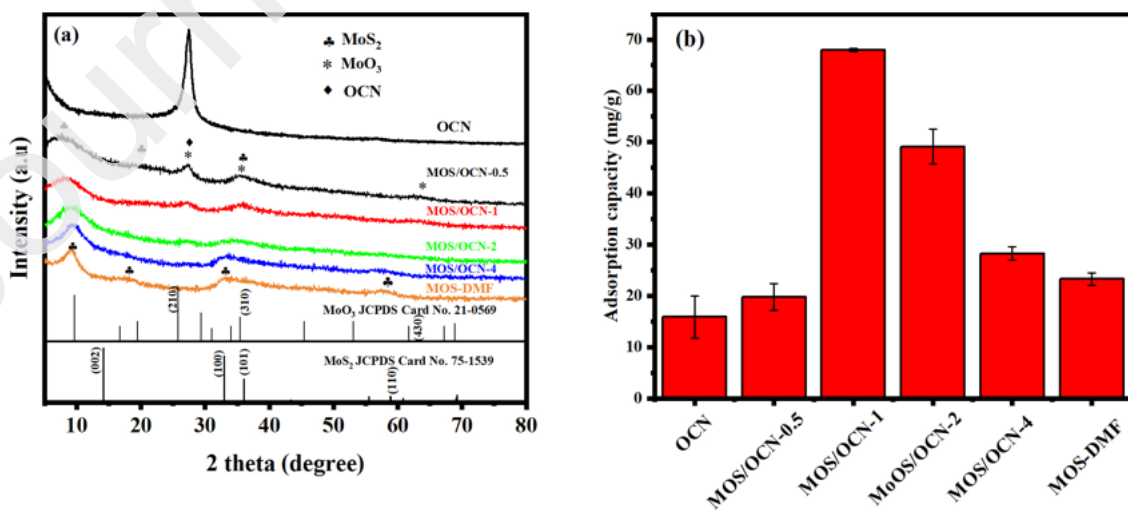
231

232 **Fig. 1**. (a) XRD patterns of synthesized adsorbents of MOS/OCN-x, MOS-DMF, and OCN; (b) Cd^{2+} adsorption

233 capacities of MOS/OCN-x, MOS-DMF and OCN. Experimental conditions: adsorbents dosage=0.25 g/L, initial

234 Cd^{2+}= 20 mg/L, pH=6.0, reaction time=24 h, temperature=25°C.

235 XPS spectra was collected to further investigate the surface properties of the synthesized

236 adsorbents (Fig. 2 and Table S2). MOS/OCN-1 was used to illustrate the typical spectra acquired

237 from analyses of MOS/OCN-x. The peak at 286.4 eV in C1s of MOS/OCN-1 (Fig.S2a) could be assigned

238 to C-O groups [30], which resulted from partial substitution of O atoms for N atoms in $g-C_3N_4$ [14].

239 In comparison, the C-O peak can be neglected in MOS-DMF due to lack of OCN in that material. The

240 peak of Mo-C (284.2 eV) or Mo-N (394.8 eV) [31] cannot be found in MOS/OCN-1. However, when

241 compared to pure OCN and physical mixed MoS_2+OCN, the slightly shift of N-C=N and C-N-H groups

242 to lower binding energies accompanied with negative shift of Mo 3p occurred in MOS/OCN-1 (Fig.

243 S2b-c). The results suggest that hydrogen bonding between OCN and Mo, S species rather than a

244 strong chemical interaction, probably existed in the heterogenous interface. Typical peaks due to

245 both Mo(IV) (229.0 eV and 232.84 eV) from MoS_2 and Mo(VI) (229.7 eV and 235.84 eV) from MoO_3

246 [25, 32, 33] were found in MOS/OCN-1 (Fig. 2a), which confirmed the coexistence of MoS_2 and MoO_3.

247 MoO_3 was likely formed by oxidization of MoS_2 on the surface of oxygen-rich OCN after Mo and S

248 hybridization, a hypothesis supported by the clearly larger peak area of MoO_3 (530.9 eV) [18] in

249 Fig.2c. As a result of MoS_2 oxidization, the peak at 168.6 eV corresponding to SO_3^{2-} [34] was also

250 observed in MOS/OCN-1 (Fig. 2b). Compared with MOS/OCN-1, much lower intensity of SO_3^{2-} and

251 MoO_3 peaks were observed in MOS-DMF when OCN was not included during the synthesis of

252 adsorbent (Fig. 2e-f). Moreover, Mo(VI) content in the absorbents (Table S2) showed a positive

253 correlation with Cd^{2+} adsorption capacity (Fig. 1b). Previous studies have demonstrated that Mo(VI)

254 also positively influenced the immobilization of other heavy metals, such as Pb^{2+} and Hg^{2+} [23, 24].

255 Hence, Mo atoms and the oxidization phenomenon may be key factors in influencing Cd^{2+}

256 adsorption.
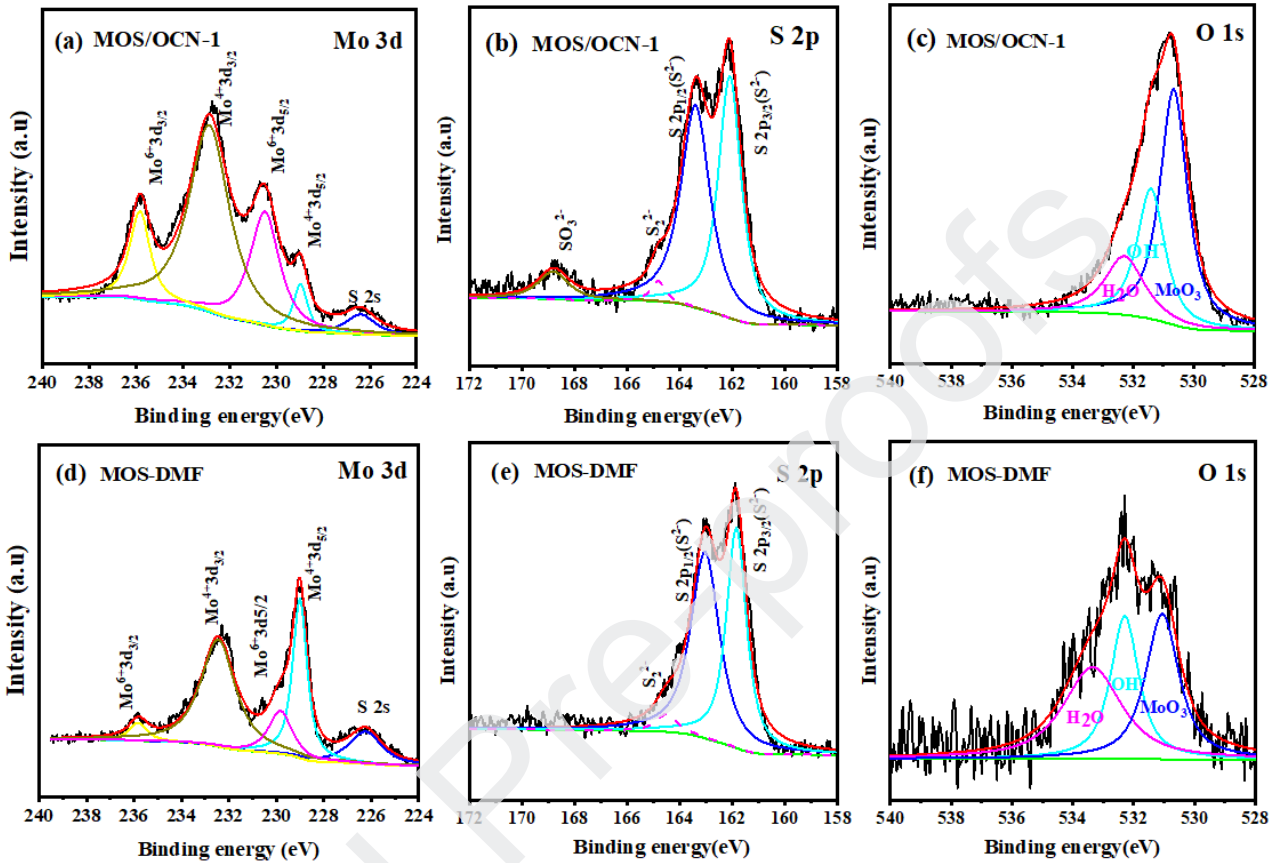
258 **Fig. 2**. XPS spectra of MOS/OCN-1: Mo 3d (a), S 2p (b) and O 1s (c). MOS-DMF: Mo 3d (d), S 2p (e) and O 1s

259 (f).

260 **3.2 Adsorption kinetics and isotherms**

261 MOS/OCN-1, as the optimum Cd^{2+} adsorbent, was selected to conduct Cd^{2+} adsorption kinetics

262 study and the results were compared with those using OCN and MOS-DMF (Fig. 3a). All three

263 adsorbents shown rapid adsorption rate during the initial stage within 10 mins but all subsequently

264 slowed down until an equilibrium was reached by 24 h. Pseudo-first order model and pseudo-

265 second order model were initially applied to simulate the kinetic data (Fig.3a and Fig.S3) and the

266 related parameters were listed in Table S3. The adsorption processes of all three adsorbents were

267 better fitted to the pseudo-second order model ($R^2 > 0.99$), which supported the premise that

268 adsorption process was dominated by chemisorption [35]. It is clear that MOS/OCN-1 performed

269 the highest capacity of 62.5 mg/g, followed by MOS-DMF (22.7 mg/g) and OCN (11.45 mg/g).

270   The results from an intraparticle diffusion model simulation (Fig. 3b) indicated that, besides

271 chemisorption, diffusion processes, especially intraparticle diffusion, may also affect the Cd^{2+}

272 adsorption rate on a solid solution interface. Data from all three adsorbents could be fitted into a

273 multi-linear plot (Fig. 3b) where the first, second and third plot portions could be ascribed to bulk

274 diffusion, intraparticle diffusion and final equilibrium, respectively [20, 36]. The slope of second plot

275 was lower than that of the initial stage, indicating that intraparticle diffusion had slowed down,

276 probably due to lower Cd^{2+} concentration after rapid boundary layer diffusion [36]. The k_{i2} value of

277 MOS/OCN-1 (0.32 mg/ g·$min^{1/2}$) was higher than that of MOS-DMF (0.29 mg/g·$min^{1/2}$) and OCN (0.07

278 mg/g·$min^{1/2}$), which can be explained by the greater dispersion of MoS_2 and MoO_3 nanosheets on

279 the surface of OCN in MOS/OCN-1, thus inducing more favourable contact of Cd^{2+} with interlayer

280 active sites. It should be noted that both the first and second linear segments (Fig. 3b) did not pass

281 through the origin, indicating that intraparticle diffusion was not the only rate-controlling step [20,

282 36] and that both surface chemical interaction and boundary layer control could have also

283 potentially affected the adsorption process.

284   The equilibrium adsorption capacity initially increased rapidly and then gradually reached

285 saturation with increasing equilibrium concentration of Cd^{2+} (Fig. 3c). Langmuir, Freundlich and Sips

286 isotherm models (Supplementary Information S1) were applied to fit the equilibrium adsorption

287 data in order to further investigate Cd^{2+} adsorption behaviour. It was obvious that the Sips isotherm

288   model possessed the best overall fit of the experimental data ($R^2 \geq 0.95$) for MOS/OCN-1, MOS-

289   DMF and OCN (Table S4). Since the Sips model is a combination of the Langmuir and Freundlich

290   models, the best fitting result with 1/n not close to unity indicated that the surfaces of the three

291   adsorbents were heterogenous [37]. For MOS-DMF and MOS/OCN-1, the heterogeneous surface

292   probably derived from multiple sites (Mo and S) active towards Cd^{2+}, while for OCN the

293   heterogenous surface might originate from pores resulting from overlapping layers [20]. By

294   calculating the maximum adsorption capacity according to the Sips isotherm equation, MOS/OCN-

295   1 exhibited the highest maximum adsorption capacity of 293.8 mg/g, which was 2.1 times and 8.7

296   times higher than MOS-DMF and OCN, respectively. Additionally, MOS/OCN-1 showed better Cd^{2+}

297   adsorption performance when comparing with the adsorption capacity (9.9-205 mg/g) of other

298   carbon-based materials or hybridized composites (Table 1). By considering the relatively low cost of

299   MOS/OCN-1 (4,970 $/kg Cd removal) compared with other materials (4,159-35,261 $/kg Cd removal)

300   (Table S5), it can be concluded that MOS/OCN-1 can act as a low-cost and high-efficiency adsorbent

301   for Cd^{2+} remediation.

302

Fig. 3. Cd^{2+} adsorption kinetics fitted with the pseudo-second order model (a) and intraparticle diffusion

model (b). Experimental condition: adsorbents dosage= 0.25 g/L, initial Cd^{2+}=20 mg/L, pH=6.0 ± 0.2,

temperature=25°C. Cd^{2+} adsorption isotherm curve fitted with Langmuir, Freundlich and Sips model (c).

Experimental conditions: adsorbents dosage=0.25 g/L, initial Cd^{2+}=15-600 mg/L, pH=6.0 ± 0.2, reaction

time=24h, temperature=25°C.

308 **Table 1**

309 Comparison of maximum Cd^{2+} adsorption capacities by different adsorbents.

Adsorbent	q_m (mg/g)	Reference
g-C_3N_4	112.4	[9]
2D –g-C_3N_4	94.4	[6]
B-doped g-C_3N_4	159.2	[38]
Fe_3O_4-g-C_3N_4	204.5	[39]
Disulfide linked polymer networks (COP 63)	9.9	[40]

TCB-700 (biologically modified biochar)	173.4	[41]
OCN	33.9	This work
MOS-DMF	139.4	This work
MOS/OCN-1	293.8	This work

310   **3.3 Influences of pH and competing ions on Cd^{2+} adsorption**

311   Cd^{2+} contaminated water is always found to exist under the acid condition with pH value

312   ranges from 2-6 [42-45]. To further evaluate the effect of pH on Cd^{2+} adsorption by MOS/OCN-1,

313   the adsorption capacity was determined separately under these conditions (Fig. 4a). The result

314   suggested that Cd^{2+} adsorption by MOS/OCN-1 improved with increasing pH. In strong acid

315   conditions, such as pH of 2 or 3, the uptake amount of Cd^{2+} by MOS/OCN-1 (<10 mg/g) was much

316   lower than that at pH 6 (63 mg/g), which may be ascribed to strong electrostatic repulsion between

317   the surface of the adsorbent and Cd^{2+} when large amounts of H$^+$ were present in solution [20]. The

318   inhibiting effect of H$^+$ reduced under the increased pH condition, thus Cd^{2+} could approach easily to

319   the surface of the adsorbent for further reaction.

320   Ca^{2+} and Mg^{2+}, as common ions in natural and wastewater, may have adverse effects on Cd^{2+}

321   adsorption due to competition in occupying the active sites in adsorbents [46]. Moreover, Zn^{2+} has

322   a similar hydrated ion radius (4.30 Å) to Cd^{2+} (4.26 Å) which may also inhibit Cd^{2+} adsorption [47].

323   Therefore, competition adsorption experiments, with different mass ratios of Ca^{2+}, Mg^{2+}, Zn^{2+} to

324   Cd^{2+} (1:1, 5:1, 10:1) were performed in order to determine their effects on Cd^{2+} adsorption. The

325   result in Fig. 4b illustrated that the adsorption efficiency of Cd^{2+} still remained 98.5% when both

326   Ca^{2+} and Mg^{2+} concentrations were up to 100 mg/L. The presence of Zn^{2+} at a concentration of 100

327   mg/L only produced a slight decreased efficiency from 99.2% to 94.6%. Thus, the three coexisting

328   ions, Ca^{2+}, Mg^{2+}, and Zn^{2+}, produced a negligible effect on Cd^{2+} adsorption by MOS/OCN-1. By

329   calculating the distribution coefficient K$_d$ (mL/g) of MOS/OCN-1 for each cation, it can be found that

330 the K_d^{Cd} value (~10^5 mL/g) in the mixed solution with cation ions of 10 mg/L was 2-3 order of

331 magnitudes higher than K_d^{Zn}, K_d^{Mg}, and K_d^{Ca} (Table S6). Since a material with a K_d value >10^4 mL /g

332 can be considered as an excellent adsorbent with high preference towards the targeted pollutant

333 [26], this result further reflecting the high affinity and selectivity of MOS/OCN-1 for Cd^{2+} over Ca^{2+},

334 Mg^{2+} and Zn^{2+}.
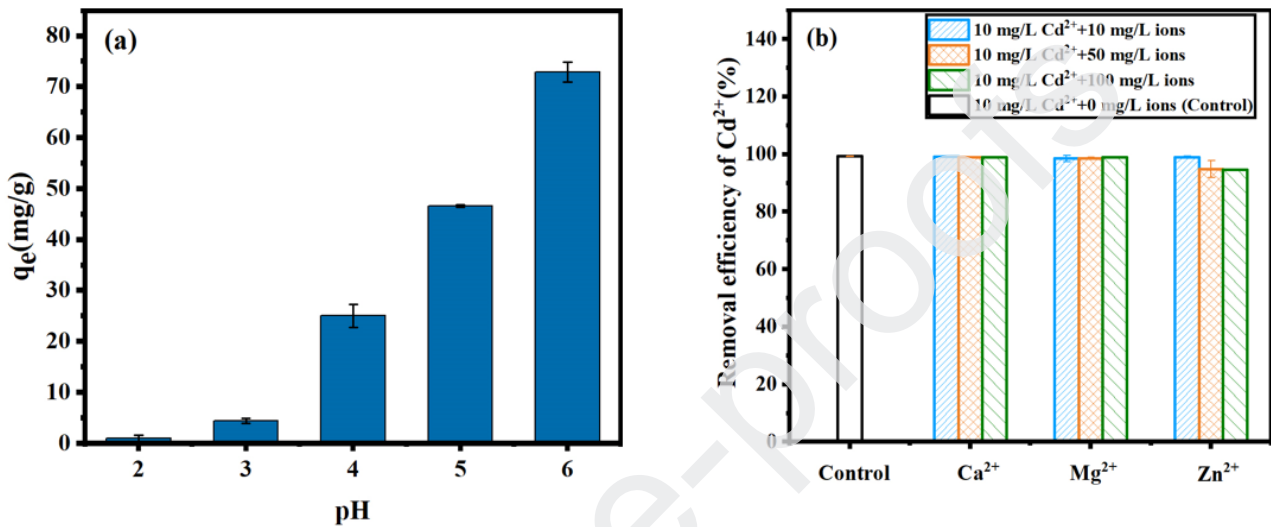
335

336 **Fig. 4**. (a). The effect of pH on Cd^{2+} removal by MOS/OCN-1. Experimental condition: adsorbents dosage=

337 0.25 g/L, initial Cd^{2+}=20 mg/L, temperature= 25°C. (b) The effect of competing ions, i.e. Ca^{2+}, Mg^{2+} and Zn^{2+}

338 on Cd^{2+} adsorption by MOS/OCN-1. Experimental conditions: adsorbents dosage=0.25 g/L, initial Cd^{2+}=10

339 mg/L, pH=6.0 ± 0.2, reaction time=24 h, temperature=25°C.

340 **3.4 Mechanisms of Cd^{2+} adsorption on MOS/OCN**

341 **3.4.1 The change of structure and composition of MOS/OCN-1**

342 XRD and XPS spectra of MOS/OCN-1 were analyzed before and after Cd^{2+} adsorption in order

343 to elucidate possible adsorption mechanisms. The XRD patterns (Fig. 5a) exhibited several new

344 peaks located at 29.21°, 31.96°, 34.80°, 47.94°, 49.99°, 55.26°, 58.97°, 60.59° and 77.78°after Cd^{2+}

345 adsorption and these peaks can be well assigned as $CdMoO_4$ (JCPDS card No. 07-0209), which

346 indicated a new precipitate $CdMoO_4$ had formed on the surface of MOS/OCN-1. From the results of

347 survey spectra by XPS (Fig. S4 and Table S7), the contents of total O and Mo significantly decreased

348 after adsorption, suggesting that Mo atoms were dissociated from the adsorbents surface, probably

349 in the form of free molybdate ions (ie. MoO_4^{2-}) [22]. Interestingly, the relative content of Mo (IV)

350 decreased from 64.2% to 57.1% after adsorption while Mo (VI) increased from 35.8% to 42.9% (Fig.

351 5b and Table S7), implying that Mo (IV) was oxidized to Mo (VI) during the adsorption process.

352 Moreover, a new peak located at 163.5eV emerged in the S 2p spectra (Fig. 5c) after adsorption,

353 suggesting the formation of CdS species [20]. However, the characteristic peaks of CdS in the XRD

354 pattern was too weak to be found, which may be ascribed to the low content.

355   From FTIR analysis (Fig. 5d), the intensity of Mo-OH, located at 881 cm^{-1}[46], decreased

356 significantly after Cd^{2+} adsorption, which suggested that surface oxygen probably dissociated from

357 the adsorbent as MoO_4^{2-}. A redshift in the Mo-O band, from 743 to 766 cm^{-1}, occurred after

358 adsorption, implying that Cd^{2+} interacted with Mo-O-Mo during adsorption [48, 49] and that was in

359 accordance with the production of $CdMoO_4$ (Fig.5a). Because of the low content of CdS, no

360 characteristic peak of Cd-S at around 630 cm^{-1} [50] was found and the peak of Mo-S (500 cm^{-1}) [51]

361 did not change noticeably after Cd^{2+} loading. However, evidence from the XPS spectra suggested

362 that Cd-S interaction also occurred during Cd^{2+} removal. Therefore, combining the results from XRD,

363 XPS and FTIR analyses, it was considered that the formation of $CdMoO_4$ precipitate as well as Cd-S

364 interaction contributed to Cd^{2+} removal by MOS/OCN-1, while the former precipitation showed

365 more obvious evidence.

366
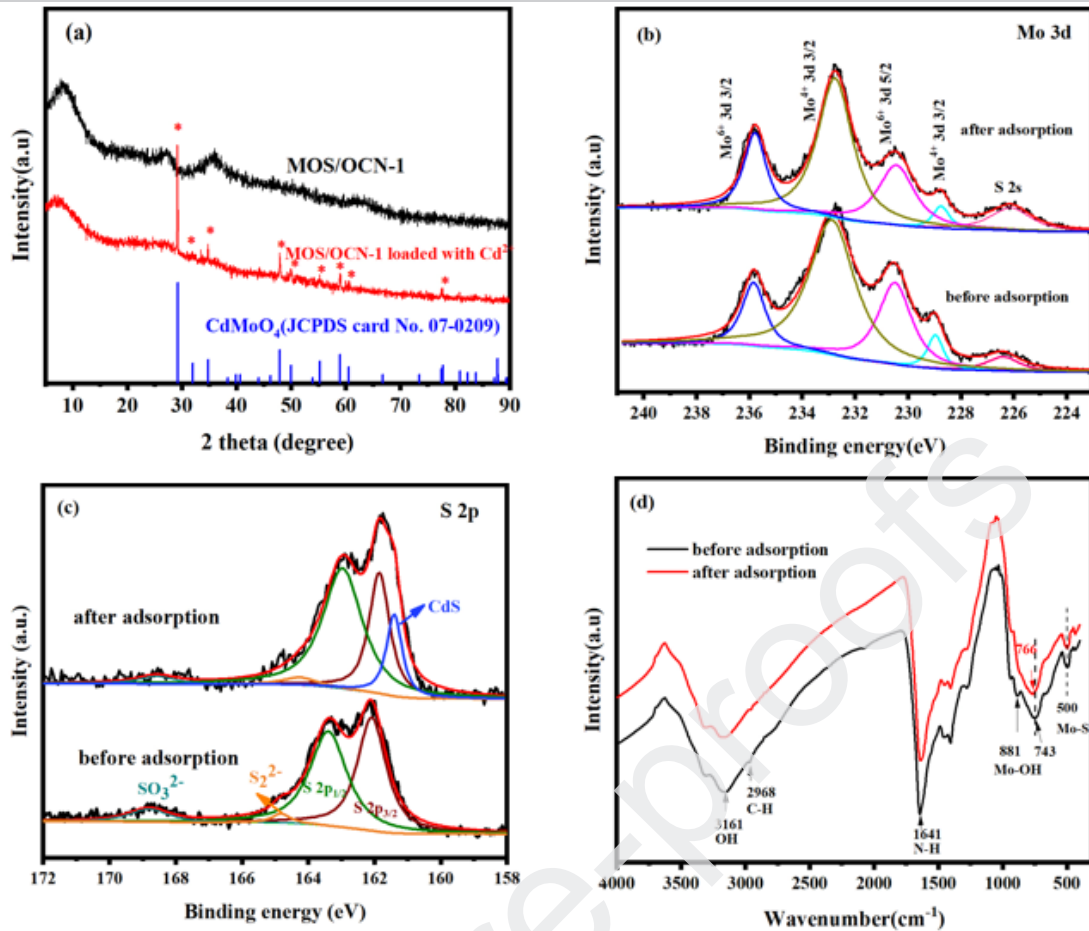
367

Fig. 5. XRD pattern of MOS/OCN-1 before and after Cd^{2+} adsorption (a). XPS spectra of Mo 3d (b) and S 2p (c)

before and after Cd^{2+} adsorption. FTIR spectra of MOS/OCN-1 before and after adsorption (d). Experimental

conditions: adsorbents dosage=1 g/L, initial Cd^{2+}=200 mg/L, pH=6.0 ± 0.2, reaction time=24 h,

temperature=25°C.

3.4.2 MoO_4^{2-} generation and contribution

In order to identify the production of MoO_4^{2-} and its effect on Cd^{2+} removal, the released

MoO_4^{2-} in solution was detected at the end of the adsorption experiment under different pH

conditions (Fig. 6). The concentration of MoO_4^{2-} in the control solution (without Cd^{2+} addition) was

found to be higher than that in the solution with 20 mg/L Cd^{2+} under all pH conditions (pH 2-6),

suggesting that the proportion of free MoO_4^{2-} combined with Cd^{2+} to form precipitate. With pH

378 increasing from 3 to 6, the concentrations of MoO_4^{2-} and total sulphur in solution gradually

379 increased, accompanied by increasing Cd^{2+} adsorption efficiency (Fig. 1b). This result can be

380 explained by two aspects. Due to the coexistence of MoS_2 and MoO_3 in the MOS/OCN-1 (Fig. 1 and

381 2), the oxidation of MoS_2 (Equation 4) and hydrolysis of MoO_3 (Equation 5) can simultaneously

382 generate MoO_4^{2-} in the solution [22, 52]. The released MoO_4^{2-} could then contribute to Cd^{2+}

383 precipitation by forming $CdMoO_4$ (Equation 6). As the release of H^+ (Equation 4 and 5) would

384 decrease the pH value during Cd^{2+} adsorption (supported by the fact that pH decreased from 6.0 to

385 4.7 if without any adjustment), therefore, extra OH^- was added into the solution to maintain the

386 targeted pH level of the solution. The addition of OH^- then drove the production of more MoO_4^{2-} for

387 Cd^{2+} removal. Additionally, the corrosion of MoS_2 with the addition of OH^- also produced dissolved

388 sulfur (S^{2-}, HS^- and SO_4^{2-} , etc) and the dissociated S(II) also led to the formation of CdS species

389 (Equation 7), which caused a decrease in dissolved sulphur in Cd^{2+} solution (insert in Fig.6). At pH 2,

390 the concentration of MoO_4^{2-} was little higher than that at pH 3, probably because MoS_2 was partly

391 dissolved in the strongly acidic condition. Further investigation showed that more dissolved MoO_4^{2-}

392 was produced during Cd^{2+} removal by MOS/OCN-1 than MOS-DMF (Fig. S5). Combined with the

393 results of FESEM imaging (Fig.S1), it can be concluded that OCN facilitated active sites exposure on

394 the adsorbent, which further led to better contact of Mo (IV)/Mo (VI) with O_2 and OH^-, thus

395 promoting the production of MoO_4^{2-} and facilitating the precipitation process.
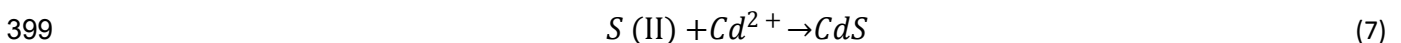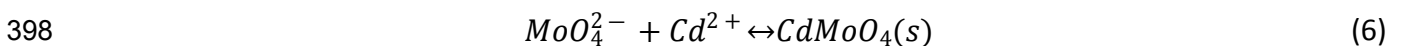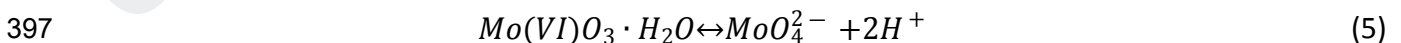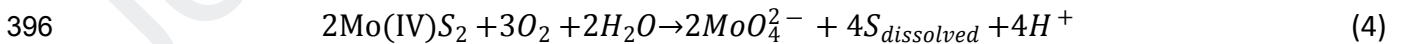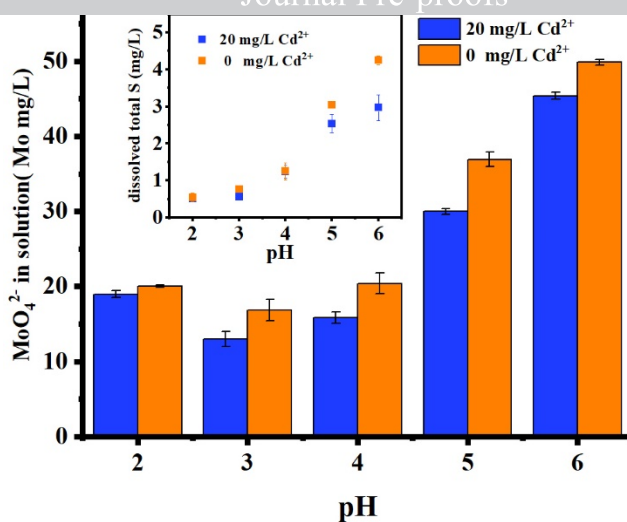
396 $$2Mo(IV)S_2 + 3O_2 + 2H_2O \rightarrow 2MoO_4^{2-} + 4S_{dissolved} + 4H^+ \tag{4}$$

397 $$Mo(VI)O_3 \cdot H_2O \leftrightarrow MoO_4^{2-} + 2H^+ \tag{5}$$

398 $$MoO_4^{2-} + Cd^{2+} \leftrightarrow CdMoO_4(s) \tag{6}$$

399 $$S\,(II) + Cd^{2+} \rightarrow CdS \tag{7}$$

Fig.6. The concentration of MoO_4^{2-} and dissolved total S after Cd^{2+} adsorption by MOS/OCN-1 under different pH conditions. Experimental conditions: adsorbents dosage=0.25 g/L, initial Cd^{2+}=20 mg/L, reaction time=24 h, temperature=25°C.

3.4.3 The role of Mo (IV) and Mo (VI) on Cd^{2+} removal

To further evaluate the contributions of MoS_2 oxidation (Equation 4) and MoO_3 hydroxylation (Equation 5) to Cd^{2+} removal, a MoO_3/OCN hybrid composite was prepared (Fig.S6) and the adsorption performance was compared to that of MOS/OCN-1. In Fig.7a, it may be observed that MoO_3/OCN exhibited a worse adsorption performance than MOS/OCN-1 with a capacity of only 20 mg/g, even though there were more Mo(VI) present in MoO_3/OCN (Fig.S7). A similar poor adsorption efficiency from pure MoO_3 has also been reported in a previous study [23]. It should be noted that the dissolved MoO_4^{2-} from MoO_3/OCN was significantly lower than that from MOS/OCN-1 in both pure water and in Cd^{2+} solution (Fig. 7b), which indicated that production of MoO_4^{2-} from MoO_3 hydrolyzation still limited in acidic condition, due to the relatively low hydrolysis constant value of MoO_3 (Ka=$10^{-11.923}$~$10^{-18.84}$) [53]. However, for MOS/OCN-1, besides intrinsic MoO_3 hydrolyzation, Mo(IV) oxidation in hybrid composite might also contribute greatly to produce more

416 MoO_4^{2-}. MoO_4^{2-} produced during the treatment by MOS/OCN-1 caused rapid precipitation of Cd^{2+}

417 on the surface of OCN, thus giving rise to better removal efficiency.
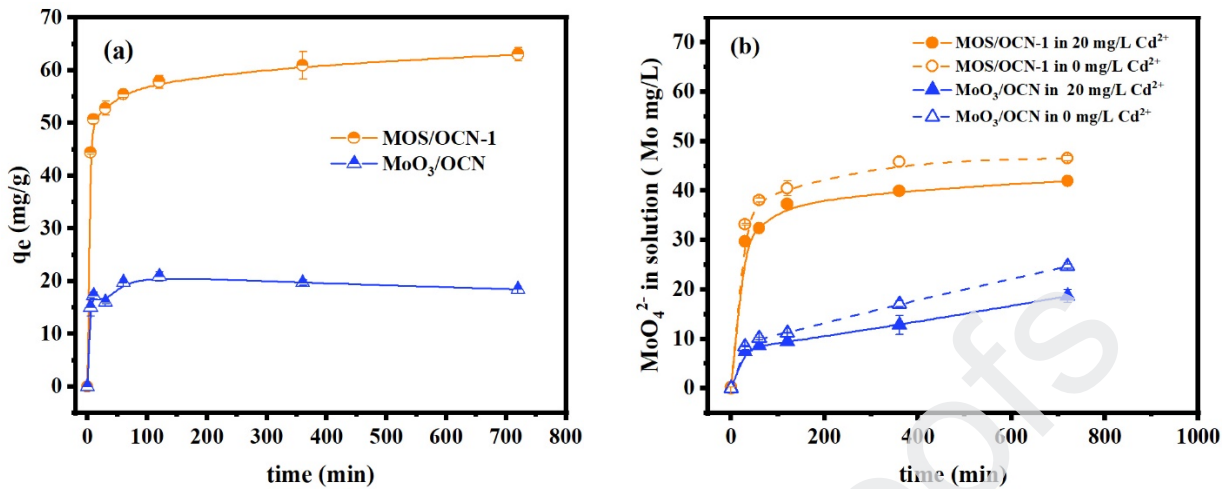
418

419 **Fig.7**. (a) Cd^{2+} adsorption performance by MOS/OCN-1 and MoO_3/OCN. (b) Free molybdate ions in Cd^{2+}

420 solution and pure water treated by MOS/OCN-1 and MoO_3/OCN. Experimental conditions: adsorbents

421 dosage = 0.25 g/L, initial Cd^{2+}=20 mg/L, pH=6.0 ± 0.2, reaction time=12 h, temperature=25°C.

422 It should be noted that the adsorption efficiency of MOS/OCN-1 decreased from 99.2% to 65.3%

423 after three times recycling (Fig. S8), which may due to the loss of Mo, S active species (Fig. 6).

424 Meanwhile, the chemical structures of MOS/OCN-1 may also be altered after several sorption-

425 desorption cycles, because the desorption process involved the use of acid substance HNO_3, which

426 could react with $CdMoO_4$ and CdS found on the surface of the adsorbent [54, 55]. Nevertheless,

427 considering the high-efficiency and relatively low-cost of MOS/OCN, MOS/OCN-1 might still showed

428 a potential in *in-situ* Cd^{2+} remediation.

429 Above all, the adsorption process of Cd^{2+} on hybrid adsorbents can be summarised as follows.

430 The oxidation of MoS_2 and the hydrolyzation of MoO_3 on OCN played a significant role for Cd^{2+}

431 removal by producing MoO_4^{2-}, which in turn precipitated Cd^{2+}. In the meantime, the dissolved S (II)

432 from the oxidized MoS_2 also interacted with Cd^{2+} by forming CdS species. Herein, OCN functioned

433 as a stable interface with large surface area to expose more active species/sites (Mo (IV)，Mo(VI)

434 and S (II)) to interact with Cd^{2+}, which finally induced the enhancement of Cd^{2+} removal.

435 **4．Conclusions**

436   In this work, Mo and S were simultaneously introduced on oxygen-doped carbon nitride (OCN)

437 through a facile one-step solvothermal process. The hybrid composite MOS/OCN-1 achieved

438 enhanced performance for Cd^{2+} removal with a maximum adsorption capacity of 293.8 mg/g, 8.7

439 times higher than that of OCN alone and superior to many other carbon-based materials. Cd^{2+}

440 adsorption followed a pseudo-second order model and the fitting to an intraparticle diffusion model

441 indicated that chemical interaction and particle diffusion process controlled the adsorption rate.

442 Moreover, good anti-interference ability towards Cd^{2+} under the presence of different coexisting

443 ions like Ca^{2+}, Mg^{2+}, Zn^{2+} was also achieved by MOS/OCN-1. OCN provided a large surface area and

444 functioned as an interface to inhibit the agglomeration of MoS_2 and MoO_3 nanoparticles, which

445 acted to expose more active sites for Cd^{2+} effective adsorption. Besides the well-known soft-soft Cd-

446 S interaction, the production of $CdMoO_4$ also contributed greatly to Cd^{2+} removal, where the release

447 of MoO_4^{2-} was controlled both by the dissociation of intrinsic Mo(VI) and oxidization of Mo(IV). This

448 work has highlighted a potential, effective and low-cost adsorbent suitable for *in-situ* Cd^{2+}

449 remediation, and has suggested related mechanisms, especially the effect of Mo atoms on the

450 adsorption process. Further studies on the general treatment capabilities of MOS/OCN for other

451 heavy metals, or those capabilities of other layered-structure materials with Mo and S modifications,

452 will be conducted in the future.

453

References

460   [1] Q. Zhou, B. Liao, L. Lin, W. Qiu, Z. Song, Adsorption of Cu(II) and Cd(II) from aqueous solutions by ferromanganese
461   binary oxide-biochar composites, Sci Total Environ, 615 (2018) 115-122.

462   [2] L. Liu, Q. Peng, G. Qiu, J. Zhu, W. Tan, C. Liu, L. Zheng, Z. Dang, Cd^{2+} adsorption performance of tunnel-structured
463   manganese oxides driven by electrochemically controlled redox, Environmental pollution, 244 (2019) 783-791.

464   [3] C. Zhang, Z. Yu, G. Zeng, B. Huang, H. Dong, J. Huang, Z. Yang, J. Wei, L. Hu, Q. Zhang, Phase transformation of
465   crystalline iron oxides and their adsorption abilities for Pb and Cd, Chemical Engineering Journal, 284 (2016) 247-259.

466   [4] T. Priya, N. Dhanalakshmi, S. Thennarasu, N. Thinakaran, A novel voltammetric sensor for the simultaneous detection
467   of Cd^{2+} and Pb^{2+} using graphene oxide/kappa-carrageenan/l-cysteine nanocomposite, Carbohydr Polym, 182 (2018) 199-
468   206.

469   [5] W.W. Tang, G.M. Zeng, J.L. Gong, J. Liang, P. Xu, C. Zhang, B.B. Huang, Impact of humic/fulvic acid on the removal of
470   heavy metals from aqueous solutions using nanomaterials: a review, Sci Total Environ, 468-469 (2014) 1014-1027.

471   [6] X. Cai, J. He, L. Chen, K. Chen, Y. Li, K. Zhang, Z. Jin, J. Liu, C. Wang, X. Wang, L. Kong, J. Liu, A 2D-g-C_3N_4 nanosheet as
472   an eco-friendly adsorbent for various environmental pollutants in water, Chemosphere, 171 (2017) 192-201.

473   [7] J.H. Park, Y.S. Ok, S.H. Kim, J.S. Cho, J.S. Heo, R.D. Delaune, D.C. Seo, Competitive adsorption of heavy metals onto
474   sesame straw biochar in aqueous solutions, Chemosphere, 142 (2016) 77-83.

475   [8] C. Liu, S. Dong, Y. Chen, Enhancement of visible-light-driven photocatalytic activity of carbon plane/g-C_3N_4/TiO_2
476   nanocomposite by improving heterojunction contact, Chemical Engineering Journal, 371 (2019) 706-718.

477   [9] C. Shen, C. Chen, T. Wen, Z. Zhao, X. Wang, A. Xu, Superior adsorption capacity of g-C_3N_4 for heavy metal ions from
478   aqueous solutions, J Colloid Interface Sci, 456 (2015) 7-14.

479   [10] R. Kumar, M.A. Barakat, F.A. Alseroury, Oxidized g-C_3N_4/polyaniline nanofiber composite for the selective removal
480   of hexavalent chromium, Scientific reports, 7 (2017) 12850.

481   [11] D. Peng, W. Jiang, F.-F. Li, L. Zhang, R.-P. Liang, J.-D. Qiu, One-Pot Synthesis of Boron Carbon Nitride Nanosheets for
482   Facile and Efficient Heavy Metal Ions Removal, ACS Sustainable Chemistry & Engineering, 6 (2018) 11685-11694.

483   [12] X.W. Yidong Zou, Yuejie Ai, Yunhai Liu, Yongfei Ji, Hongqing Wang, Tasawar Hayat, Ahmed Alsaedi, Wenping Hu and
484   Xiangke Wang, β-Cyclodextrin modified graphitic carbon nitride for the removal of pollutants from aqueous solution:
485   experimental and theoretical calculation study, Journal of Materials Chemistry A, 4 (2016) 14170-14179.

486   [13] P. Wang, L. Yin, J. Wang, C. Xu, Y. Liang, W. Yao, X. Wang, S. Yu, J. Chen, Y. Sun, X. Wang, Superior immobilization
487   of U(VI) and 243 Am(III) on polyethyleneimine modified lamellar carbon nitride composite from water environment,
488   Chemical Engineering Journal, 326 (2017) 863-874.

489   [14] P. Qiu, C. Xu, H. Chen, F. Jiang, X. Wang, R. Lu, X. Zhang, One step synthesis of oxygen doped porous graphitic carbon
490   nitride with remarkable improvement of photo-oxidation activity: Role of oxygen on visible light photocatalytic activity,
491   Applied Catalysis B: Environmental, 206 (2017) 319-327.

492   [15] L. Wang, Y. Shi, D. Yao, H. Pan, H. Hou, J. Chen, J.C. Crittenden, Cd complexation with mercapto-functionalized
493   attapulgite (MATP): Adsorption and DFT study, Chemical Engineering Journal, 366 (2019) 569-576.

[16] J. Ali, H. Wang, J. Iftikhar, A. Khan, T. Wang, K. Zhan, A. Shahzad, Z. Chen, Z. Chen, Efficient, stable and selective adsorption of heavy metals by thio-functionalized layered double hydroxide in diverse types of water, Chemical Engineering Journal, 332 (2018) 387-397.

[17] K. Ai, C. Ruan, M. Shen, L. Lu, MoS_2 Nanosheets with Widened Interlayer Spacing for High-Efficiency Removal of Mercury in Aquatic Systems, Advanced Functional Materials, 26 (2016) 5542-5549.

[18] F. Jia, Q. Wang, J. Wu, Y. Li, S. Song, Two-Dimensional Molybdenum Disulfide as a Superb Adsorbent for Removing Hg^{2+} from Water, ACS Sustainable Chemistry & Engineering, 5 (2017) 7410-7419.

[19] M. Zhang, F. Jia, M. Dai, S. Song, Combined electrosorption and chemisorption of low concentration Pb(II) from aqueous solutions with molybdenum disulfide as electrode, Applied Surface Science, 455 (2018) 258-266.

[20] Q. Wang, L. Yang, F. Jia, Y. Li, S. Song, Removal of Cd (II) from water by using nano-scale molybdenum disulphide sheets as adsorbents, Journal of Molecular Liquids, (2018).

[21] F. Jia, X. Zhang, S. Song, AFM study on the adsorption of Hg^{2+} on natural molybdenum disulfide in aqueous solutions, Phys Chem Chem Phys, 19 (2017) 3837-3844.

[22] X. Zhang, F. Jia, B. Yang, S. Song, Oxidation of Molybdenum Disulfide Sheet in Water under in Situ Atomic Force Microscopy Observation, The Journal of Physical Chemistry C, 121 (2017) 9938-9943.

[23] Y. Wu, X. Cheng, X. Zhang, Y. Xu, S. Gao, H. Zhao, L. Huo, High efficient and selective removal of Pb^{2+} through formation of lead molybdate on alpha-MoO_3 porous nanosheets array, J Colloid Interface Sci, 491 (2017) 80-88.

[24] F. Jia, C. Liu, B. Yang, X. Zhang, H. Yi, J. Ni, S. Song, Thermal Modification of the Molybdenum Disulfide Surface for Tremendous Improvement of Hg^{2+} Adsorption from Aqueous Solution, ACS Sustainable Chemistry & Engineering, 6 (2018) 9065-9073.

[25] H. Liu, X. Chen, L. Deng, M. Ding, J. Li, X. He, Perpendicular growth of few-layered MoS_2 nanosheets on MoO_3 nanowires fabricated by direct anion exchange reactions for high-performance lithium-ion batteries, Journal of Materials Chemistry A, 4 (2016) 17764-17772.

[26] M.L. Feng, D. Sarma, X.H. Qi, K.Z. Du, X.Y. Huang, M.G. Kanatzidis, Efficient Removal and Recovery of Uranium by a Layered Organic-Inorganic Hybrid Thiostannate, J Am Chem Soc, 138 (2016) 12578-12585.

[27] J. Xie, J. Zhang, S. Li, F. Grote, X. Zhang, H. Zhang, R. Wang, Y. Lei, B. Pan, Y. Xie, Controllable disorder engineering in oxygen-incorporated MoS_2 ultrathin nanosheets for efficient hydrogen evolution, J Am Chem Soc, 135 (2013) 17881-17888.

[28] M.-h. Wu, L. Li, Y.-c. Xue, G. Xu, L. Tang, N. Liu, W.-y. Huang, Fabrication of ternary GO/g- C_3N_4 /MoS_2 flower-like heterojunctions with enhanced photocatalytic activity for water remediation, Applied Catalysis B: Environmental, 228 (2018) 103-112.

[29] S. Kizito, H. Luo, S. Wu, Z. Ajmal, T. Lv, R. Dong, Phosphate recovery from liquid fraction of anaerobic digestate using four slow pyrolyzed biochars: Dynamics of adsorption, desorption and regeneration, Journal of Environmental Management, 201 (2017) 260-267.

[30] A. Zhu, L. Qiao, P. Tan, W. Zeng, Y. Ma, R. Dong, J. Pan, Boosted electrocatalytic activity of nitrogen-doped porous carbon triggered by oxygen functional groups, J Colloid Interface Sci, 541 (2019) 133-142.

[31] Y.-I. Song, J.-T. Ren, G. Yuan, Y. Yao, X. Liu, Z.-Y. Yuan, Facile synthesis of Mo_2C nanoparticles on N-doped carbon nanotubes with enhanced electrocatalytic activity for hydrogen evolution and oxygen reduction reactions, Journal of Energy Chemistry, 38 (2019) 68-77.

[32] Q. Gu, H. Sun, Z. Xie, Z. Gao, C. Xue, MoS2-coated microspheres of self-sensitized carbon nitride for efficient photocatalytic hydrogen generation under visible light irradiation, Applied Surface Science, 396 (2017) 1808-1815.

[33] M. Wu, J. Zhan, K. Wu, Z. Li, L. Wang, B. Geng, L. Wang, D. Pan, Metallic 1T MoS_2 nanosheet arrays vertically grown on activated carbon fiber cloth for enhanced Li-ion storage performance, J. Mater. Chem. A, 5 (2017) 14061-14069.

[34] W.-H. Hu, X. Shang, J. Xue, B. Dong, J.-Q. Chi, G.-Q. Han, Y.-R. Liu, X. Li, K.-L. Yan, Y.-M. Chai, C.-G. Liu, Activating MoS_2/CNs by tuning (001) plane as efficient electrocatalysts for hydrogen evolution reaction, International Journal of

539 Hydrogen Energy), 42 (2017) 2668-2685.

540 [35] L. Ma, Q. Wang, S.M. Islam, Y. Liu, S. Ma, M.G. Kanatzidis, Highly Selective and Efficient Removal of Heavy Metals
541 by Layered Double Hydroxide Intercalated with the MoS_4^{2-} Ion, J Am Chem Soc, 138 (2016) 2858-2866.

542 [36] T. Liu, S. Zheng, L. Yang, Magnetic zirconium-based metal-organic frameworks for selective phosphate adsorption
543 from water, J Colloid Interface Sci, 552 (2019) 134-141.

544 [37] G.G. Haciosmanoglu, T. Dogruel, S. Genc, E.T. Oner, Z.S. Can, Adsorptive removal of bisphenol A from aqueous
545 solutions using phosphonated levan, Journal of hazardous materials, 374 (2019) 43-49.

546 [38] G. Tan, Z. Li, H. Yuan, D. Xiao, Sorption of Cadmium from Aqueous Solution with a Highly Effective Sorbent – B-
547 Doped g-C_3N_4, Separation Science and Technology, 49 (2014) 1566-1573.

548 [39] S. Guo, C. Zhang, F. Zhang, X. Li, P. Zhang, L. Luo, Synthesis of magnetic g-C_3N_4 by one-step method and its adsorption
549 performance for Cd(II), IOP Conference Series: Materials Science and Engineering, 274 (2017) 012091.

550 [40] D. Ko, J.S. Lee, H.A. Patel, M.H. Jakobsen, Y. Hwang, C.T. Yavuz, H.C.B. Hansen, H.R. Andersen, Selective removal of
551 heavy metal ions by disulfide linked polymer networks, Journal of hazardous materials, 332 (2017) 140-148.

552 [41] Q. Tao, Y. Chen, J. Zhao, B. Li, Y. Li, S. Tao, M. Li, Q. Li, Q. Xu, Y. Li, H. Li, B. Li, Y. Chen, C. Wang, Enhanced Cd removal
553 from aqueous solution by biologically modified biochar derived from digestion residue of corn straw silage, Sci Total
554 Environ, 674 (2019) 213-222.

555 [42] K. Brahmi, W. Bouguerra, K. Missaoui, Z. Tlili, E. Elaloui, M. Loungou, B. Hamrouni, Highly cost-effective and reuse-
556 oriented treatment of cadmium-polluted mining wastewater by electrocoagulation process, Journal of Environmental
557 Engineering, 142 (2016) 04016061.

558 [43] C. Zhou, J. Ni, D. Zhang, C. Sun, Cellulosic adsorbent functionalized with macrocyclic pyridone pentamer for
559 selectively removing metal cations from aqueous solutions, Carbohydrate Polymers, 217 (2019) 1-5.

560 [44] Z. Wu, W. Deng, W. Zhou, J. Luo, Novel magnetic polysaccharide/graphene oxide @Fe_3O_4 gel beads for adsorbing
561 heavy metal ions, Carbohydr Polym, 216 (2019) 119-128.

562 [45] J. Liu, X. Ge, X. Ye, G. Wang, H. Zhang, H. Zhou, Y. Zhang, H. Zhao, 3D graphene/δ-MnO_2 aerogels for highly efficient
563 and reversible removal of heavy metal ions, Journal of Materials Chemistry A, 4 (2016) 1970-1979.

564 [46] J. Wang, W. Zhang, X. Yue, Q. Yang, F. Liu, Y. Wang, D. Zhang, Z. Li, J. Wang, One-pot synthesis of multifunctional
565 magnetic ferrite–MoS_2–carbon dot nanohybrid adsorbent for efficient Pb(II) removal, Journal of Materials Chemistry A,
566 4 (2016) 3893-3900.

567 [47] Y. Gao, X. Ren, J. Wu, T. Hayat, A. Alsaedi, C. Cheng, C. Chen, Graphene oxide interactions with co-existing heavy
568 metal cations: adsorption, colloidal properties and joint toxicity, Environmental Science: Nano, 5 (2018) 362-371.

569 [48] L. Kong, Z. Li, X. Huang, S. Huang, H. Sun, M. Liu, L. Li, Efficient removal of Pb(II) from water using magnetic
570 Fe_3S_4/reduced graphene oxide composites, Journal of Materials Chemistry A, 5 (2017) 19333-19342.

571 [49] S. Mostafa Hosseinpour-Mashkani, M. Maddahfar, A. Sobhani-Nasab, Novel silver-doped $CdMoO_4$: synthesis,
572 characterization, and its photocatalytic performance for methyl orange degradation through the sonochemical method,
573 Journal of Materials Science: Materials in Electronics, 27 (2015) 474-480.

574 [50] L. Zhang, X. Li, Z. Mu, J. Miao, K. Wang, R. Zhang, S. Chen, A novel composite of CdS nanorods growing on a
575 polyaniline-Cd^{2+} particles surface with excellent formaldehyde gas sensing properties at low temperature, RSC Advances,
576 8 (2018) 30747-30754.

577 [51] G. Angamuthu, D.B. Babu, K. Ramesha, V. Rangarajan, MoS_2 anchored carbon nitride based mesoporous material
578 as a polysulfide barrier for high capacity lithium-sulfur battery, Journal of Electroanalytical Chemistry, 843 (2019) 37-46.

579 [52] B. Mondal, A. Mahendranath, A. Som, S. Bose, T. Ahuja, A.A. Kumar, J. Ghosh, T. Pradeep, Rapid reaction of MoS_2
580 nanosheets with Pb^{2+} and Pb^{4+} ions in solution, Nanoscale, 10 (2018) 1807-1814.

581 [53] T.P. Dadze, G.A. Kashirtseva, M.P. Novikov, A.V. Plyasunov, Solubility of calcium molybdate in aqueous solutions at
582 573 K and thermodynamics of monomer hydrolysis of Mo(VI) at elevated temperatures, Monatshefte für Chemie -
583 Chemical Monthly, 149 (2017) 261-282.

584 [54] Z. Fang, Z. Li, Z. Qu, H. Xu, J. Xu, N. Yan, A novel method for the sequential removal and separation of multiple heavy

585 metals from wastewater, Journal of hazardous materials, 342 (2018) 617-624.

586 [55] W.-S. Wang, L. Zhen, C.-Y. Xu, W.-Z. Shao, Z.-L. Chen, Formation of $CdMoO_4$ porous hollow nanospheres via a self-

587 assembly accompanied with Ostwald ripening process and their photocatalytic performance, CrystEngComm, 15 (2013).

588

589 **Figure captions**

590 **Fig. 1**. (a) XRD patterns of synthesized adsorbents of MOS/OCN-x, MOS-DMF, and OCN; (b) Cd^{2+} adsorption

591 capacities of MOS/OCN-x, MOS-DMF and OCN. Experimental conditions: adsorbents dosage=0.25 g/L, initial

592 Cd^{2+}= 20 mg/L, pH=6.0, reaction time=24 h, temperature=25°C.

593 **Fig.2.** XPS spectra of MOS/OCN-1: Mo 3d (a), S 2p (b) and O 1s (c). MOS-DMF: Mo 3d (d), S 2p (e) and O 1s

594 (f).

595 **Fig. 3**. Cd^{2+} adsorption kinetics fitted with the pseudo-second order model (a) and intraparticle diffusion

596 model (b). Experimental condition: adsorbents dosage= 0.25 g/L, initial Cd^{2+}=20 mg/L, pH=6.0 ± 0.2,

597 temperature=25°C. Cd^{2+} adsorption isotherm curve fitted with Langmuir, Freundlich and Sips model (c).

598 Experimental conditions: adsorbents dosage=0.25 g/L, initial Cd^{2+}=15-600 mg/L, pH=6.0 ± 0.2, reaction

599 time=24h, temperature=25°C.

600 **Fig. 4**. (a). The effect of pH on Cd^{2+} removal by MOS/OCN-1. Experimental condition: adsorbents dosage=

601 0.25 g/L, initial Cd^{2+}=20 mg/L, temperature= 25°C. (b) The effect of competing ions, i.e. Ca^{2+}, Mg^{2+} and Zn^{2+}

602 on Cd^{2+} adsorption by MOS/OCN-1. Experimental conditions: adsorbents dosage=0.25 g/L, initial Cd^{2+}=10

603 mg/L, pH=6.0 ± 0.2, reaction time=24 h, temperature=25°C.

604 **Fig. 5**. XRD pattern of MOS/OCN-1 before and after Cd^{2+} adsorption (a). XPS spectra of Mo 3d (b) and S 2p (c)

605 before and after Cd^{2+} adsorption. FTIR spectra of MOS/OCN-1 before and after adsorption (d). Experimental

606 conditions: adsorbents dosage=1 g/L, initial Cd^{2+}=200 mg/L, pH=6.0 ± 0.2, reaction time=24 h,

607 temperature=25°C

608 **Fig.6.** The concentration of MoO_4^{2-} and dissolved total S after Cd^{2+} adsorption by MOS/OCN-1 under different

609 pH conditions. Experimental conditions: adsorbents dosage=0.25 g/L, initial Cd^{2+}=20 mg/L, reaction time=24

610   h, temperature=25°C.

611   **Fig.7**. (a) Cd^{2+} adsorption performance by MOS/OCN-1 and MoO$_3$/OCN. (b) Free molybdate ions in Cd^{2+}

612   solution and pure water treated by MOS/OCN-1 and MoO$_3$/OCN. Experimental conditions: adsorbents

613   dosage = 0.25 g/L, initial Cd^{2+}=20 mg/L, pH=6.0 ± 0.2, reaction time=12 h, temperature=25°C

614

615

616 **Tables**

617 **Table 1**

618 Comparison of maximum Cd^{2+} adsorption capacities by different adsorbents.

Adsorbent	q_m (mg/g)	Reference
g-C_3N_4	112.4	[9]
2D –g-C_3N_4	94.4	[6]
B-doped g-C_3N_4	159.2	[38]
Fe_3O_4-g-C_3N_4	204.5	[39]
Disulfide linked polymer networks (COP 63)	9.9	[40]
TCB-700 (biologically modified biochar)	175.4	[41]
OCN	33.9	This work
MOS-DMF	139.4	This work
MOS/OCN-1	293.8	This work

619

620